HAL open science

An Optimal Control Problem for Elastic Registration and Force Estimation in Augmented Surgery

Guillaume Mestdagh, Stéphane Cotin

To cite this version:

Guillaume Mestdagh, Stéphane Cotin. An Optimal Control Problem for Elastic Registration and Force Estimation in Augmented Surgery. MICCAI 2022 - 25th International Conference on Medical Image Computing and Computer Assisted Intervention, Sep 2022, Singapore, Singapore. 10.1007/978-3-031-16449-1_8 . hal-03691913

HAL Id: hal-03691913

https://inria.hal.science/hal-03691913v1

Submitted on 16 Jun 2022

HAL is a multi-disciplinary open access archive for the deposit and dissemination of scientific research documents, whether they are published or not. The documents may come from teaching and research institutions in France or abroad, or from public or private research centers.

L'archive ouverte pluridisciplinaire **HAL**, est destinée au dépôt et à la diffusion de documents scientifiques de niveau recherche, publiés ou non, émanant des établissements d'enseignement et de recherche français ou étrangers, des laboratoires publics ou privés.

An Optimal Control Problem for Elastic Registration and Force Estimation in Augmented Surgery

Guillaume Mestdagh and Stéphane Cotin

Inria, Strasbourg, France (stephane.cotin@inria.fr)

Abstract. The nonrigid alignment between a pre-operative biomechanical model and an intra-operative observation is a critical step to track the motion of a soft organ in augmented surgery. While many elastic registration procedures introduce artificial forces into the direct physical model to drive the registration, we propose in this paper a method to reconstruct the surface loading that actually generated the observed deformation. The registration problem is formulated as an optimal control problem where the unknown is the surface force distribution that applies on the organ and the resulting deformation is computed using an hyperelastic model. Advantages of this approach include a greater control over the set of admissible force distributions, in particular the opportunity to choose where forces should apply, thus promoting physically-consistent displacement fields. The optimization problem is solved using a standard adjoint method. We present registration results with experimental phantom data showing that our procedure is competitive in terms of accuracy. In an example of application, we estimate the forces applied by a surgery tool on the organ. Such an estimation is relevant in the context of robotic surgery systems, where robotic arms usually do not allow force measurements, and providing force feedback remains a challenge.

Keywords: Augmented surgery · Optimal control · Biomechanical simulation

1 Introduction

In the context of minimally-invasive surgery, abdominal organs are constantly subject to large deformations. These deformations, in combination with the limited visual feedback available to medical staff, make an intervention such as tumor ablation a complex task for the surgeon. Augmented reality systems have been designed to provide a three-dimensional view of an organ, which shows the current position of internal structures. This virtual view is superimposed onto intra-operative images displayed in the operating room.

Without loss of generality, we consider the case of liver laparoscopic surgery. In [8], the authors describe a full pipeline to produce augmented images. In their work, available data are intra-operative images provided by a laparoscopic

stereo camera, and a biomechanical model of the organ and its internal structures, computed from pre-operative CT scans. During the procedure, a point cloud representing the current location of the liver surface is first extracted from laparoscopic images, and then the pre-operative model is aligned with the intra-operative point cloud in a non-rigid way.

The elastic registration procedure used to perform the alignment between pre- and intra-operative data is a widely studied subject. In particular, much attention has been given to choosing an accurate direct mechanical model for the liver and its surroundings. The liver parenchyma is usually described using a hyperelastic constitutive law (see [11] for an extensive review). Used hyperelastic models include Saint-Venant-Kirchhoff [6], neo-Hookean [12] or Ogden models [15]. Due to its reduced computational cost, the linear co-rotational model [14] is a popular solution when it comes to matching a real-time performance constraint [22; 19; 18]. Additional stiffness due to the presence of blood vessels across the parenchyma is sometimes also taken into account [7]. A less discussed aspect of the modeling is the interaction between the liver and its surroundings, which results in boundary conditions applied on the liver surface. Proposed approaches often involve Dirichlet boundary conditions where the main blood vessels enter the liver [18] or springs to represent ligaments holding the organ [15].

Another key ingredient to obtain accurate reconstructions is the choice of a registration procedure. In many physics-based registration methods in the literature, fictive forces or energies are added into the direct problem to drive the registration. Approaches based on the Iterative Closest Point algorithm introduce attractive forces beetween the liver and the observed point cloud and let the system evolve as a time-dependent process toward an equilibrium [8; 19]. In [22], the authors model those attractive forces using an electrostatic potential. In [18], sliding constraints are used in the direct problem to enforce correspondence between the deformed liver model and the observed data. Such constraints are enforced by Lagrange multipliers that are also fictive forces. As the intra-operative observation is not a real protagonist of the physical model, those fictive forces do not reflect the true causes of displacements. This results in a poorly physically-consistent displacement field, regardless of the direct model. These methods cannot guarantee accurate registrations.

In this paper, we present a method to reconstruct a surface force distribution that explains the observed deformation, using the optimal control formalism. The problem formulation includes the choice of an elastic model (Section 2.1), a set of admissible forces and an objective function to minimize (Section 2.2). In particular, the set of admissible forces is specified by the direct model to ensure physically-consistent deformations. The adjoint method used to perform the optimization is described in Section 2.3.

Some existing works in the literature are concerned with reconstructing the physical causes of displacement. In [17], the effects of gravity and pneumoperitoneum pressure are taken into account to perform an initial intraoperative registration. In [20], the authors control the imposed displacement on parts of the liver boundary that are subject to contact forces, while a free boundary con-

dition is applied onto other parts. A numerical method similar to our adjoint method is used in [10] to register a liver model onto a point cloud coupled with ultrasound data. While their method is very specific and tailored for linear elasticity, we present a more generic approach which is compatible with nonlinear models. Our method is relevant when a measurement of forces is needed, in particular when the surgeon interacts with the organ through a surgical robotic system without force sensor. We give an example of such a force estimation in Section 3.2.

2 Methods

In this section, we give details about the optimal control problem formulation. We first specify some notation around the direct model, then we introduce the optimization problem. In the last part, we describe the adjoint method, which is used to compute derivatives of the objective function with respect to the control.

2.1 Hyperelastic model and observed data

The liver parenchyma in its pre-operative configuration is represented by a meshed domain Ω, filled with an elastic material. When a displacement field $\mathbf{u}$ is applied to Ω, the deformed mesh is denoted by $\Omega_{\mathbf{u}}$ and its boundary is denoted by $\partial\Omega_{\mathbf{u}}$. Note that the system state is fully known through the displacement of mesh nodes, stored in $\mathbf{u}$. The liver is embedded with a hyperelastic model. When a surface force distribution $\mathbf{b}$ is applied to the liver boundary, the resulting displacement $\mathbf{u_b}$ is the unique solution of the static equilibrium equation

$$\mathbf{F}(\mathbf{u_b}) = \mathbf{b}, \tag{1}$$

where $\mathbf{F}$ is the residual from the hyperelastic model. Note that $\mathbf{F}$ is very generic and may also account for blood vessels rigidity, gravity or other elements in a more sophisticated direct model.

The observed intra-operative surface is represented by a point cloud $\Gamma = \{y_1, \ldots, y_m\}$. We also define the orthogonal projection onto $\partial\Omega_{\mathbf{u}}$, also called the closest point operator,

$$p_{\mathbf{u}}(y) = \arg\min_{x \in \partial\Omega_{\mathbf{u}}} \|y - x\|.$$

Here, we consider that the orthogonal projection operator always returns a unique point, as points with multiple projections onto $\partial\Omega_{\mathbf{u}}$ represent a negligible subset of $\mathbb{R}^3$.

2.2 Optimization problem

We perform the registration by computing a control $\mathbf{b}$ so that the resulting displacement $\mathbf{u_b}$ is in adequation with observed data. The optimization problem reads

$$\min_{\mathbf{b} \in B} \quad \Phi(\mathbf{b}) \qquad \text{where} \qquad \Phi(\mathbf{b}) = J(\mathbf{u_b}) + R(\mathbf{b}), \tag{2}$$

where J measures the discrepancy between a prediction $\mathbf{u_b}$ and observed data, R is an optional regularization term, and B is the set of admissible controls.

The functional J enforces adequation with observed data and contains information such as corresponding landmarks between pre– and intra-operative surfaces. Many functionals of this kind exist in the literature, based on surface correspondence tools [see 21, and references therein]. In this paper, we use a simple least-squares term involving the orthogonal projection onto $\partial\Omega_{\mathbf{u}}$, which reads

$$J(\mathbf{u}) = \tfrac{1}{2m} \sum_{j=1}^{m} \|p_{\mathbf{u}}(y_j) - y_j\|^2. \tag{3}$$

The functional $J(\mathbf{u})$ evaluates to zero whenever every point $y \in \Gamma$ is matched by the deformed surface $\partial\Omega_{\mathbf{u}}$. If $\mathbf{v}$ is a perturbation of the current displacement field $\mathbf{u}$, the gradient of (3) with respect to the displacement is defined by

$$\langle \nabla J(\mathbf{u}), \mathbf{v} \rangle = \tfrac{1}{m} \sum_{j=1}^{m} \big(r_j - y_j\big) \cdot \mathbf{v}(r_j), \tag{4}$$

where $r_j = p_{\mathbf{u}}(y_j)$ and $\mathbf{v}(r_j)$ is the displacement of the point of $\partial\Omega_{\mathbf{u}}$ currently at r_j under the perturbation $\mathbf{v}$.

The set of admissible controls B contains a priori information about the surface force distribution $\mathbf{b}$, including the parts of the liver boundary where $\mathbf{b}$ is nonzero and the maximal intensity it is allowed to take. The selection of zones where surface forces apply is critical to obtain physically plausible registrations. In comparison, a spring-based approach would result in forces concentrated in zones where the spring are fixed, which might disagree with the direct model.

2.3 Adjoint method

We solve problem (2) using an adjoint method In such a method, the only optimization variable is $\mathbf{b}$. Descent directions for the objective function Φ are computed in the space of controls, which requires to compute $\nabla\Phi(\mathbf{b})$. To differentiate $J(\mathbf{u_b})$ with respect to $\mathbf{b}$, we use an adjoint state $\mathbf{p_b}$ defined as the solution of the adjoint system

$$\nabla\mathbf{F}(\mathbf{u_b})^{\mathrm{T}}\mathbf{p_b} = \nabla J(\mathbf{u_b}). \tag{5}$$

A standard calculation [see for instance 1] shows that

$$\mathbf{p_b} = \frac{\mathrm{d}}{\mathrm{d}\mathbf{b}}\left[J(\mathbf{u_b})\right] \qquad \text{and} \qquad \nabla\Phi(\mathbf{b}) = \mathbf{p} + \nabla R(\mathbf{b}).$$

The procedure to compute the objective gradient is summarized in Algorithm 1. For a given $\mathbf{b}$, evaluating $\Phi(\mathbf{b})$ and $\nabla\Phi(\mathbf{b})$ requires to solve the direct problem, and then to assemble and solve the adjoint problem, which is linear. In other words, the additional cost compared to a direct simulation is that of solving one linear system. The resulting gradient is then fed to a standard gradient-based optimization algorithm to solve (2) iteratively.

Algorithm 1: Computation of objective gradient using an adjoint method.

Data: Current iterate $\mathbf{b}$
Compute the displacement $\mathbf{u_b}$ by solving (1)
Evaluate $\nabla J(\mathbf{u_b})$ and $\nabla \mathbf{F}(\mathbf{u_b})$
Compute the adjoint state $\mathbf{p_b}$ by solving (5)
Result: $\nabla \Phi(\mathbf{b}) = \mathbf{p_b} + \nabla R(\mathbf{b})$

3 Results

Our method is implemented in Python (Numpy and Scipy), and we use a limited-memory BFGS algorithm [4] as an optimization procedure. Our numerical tests run on an Intel Core i7-8700 CPU at 3.20 GHz with 16 GB RAM.

3.1 Sparse Data Challenge dataset

To evaluate our approach in terms of displacement accuracy, we use the Sparse Data Challenge[1] dataset. It consists of one tetrahedral mesh representing a liver phantom in its initial configuration and 112 point clouds acquired from deformed configurations of the same phantom [5; 3]. Once the registration is done, the final position of the mesh nodes for each point cloud is uploaded on the challenge website. Then the target registration error (TRE) is computed, using 159 targets whose positions are unknown to us.

Before we begin the elastic registration process, we use the standard Iterative Closest Point method [2] to perform a rigid alignment. Then we set a fixed boundary condition on a small zone of the posterior face to enforce the uniqueness of the solution to the direct elastic problem. As the liver mesh represents a phantom, no information about blood vessels is available and for this reason we just choose six adjacent triangles close to the center of the posterior face to apply the fixed displacement constraint. As specified by the challenge authors, the forces causing the deformation are contact forces applied onto the posterior face of the phantom, while the point cloud was acquired by observing the anterior surface. As a consequence, we label the anterior surface as the "matching surface", which is to be matched with the point cloud, while the posterior surface is labeled as "loaded surface", where the force distribution $\mathbf{b}$ is allowed to take nonzero values. Figure 1 shows the initial mesh with the matching and loaded surfaces in different colors, a point cloud and the liver mesh after rigid registration. In a clinical context, the surface in the field of view of the camera may be labeled as the matching surface while forces are allowed on the remaining hidden surface.

We solve problem (2) (with $R(\mathbf{b}) = 0$) using the adjoint method presented in Section 2.3. As only small deformations are involved in this dataset, we use

[1] See details and results at sparsedatachallenge.org.

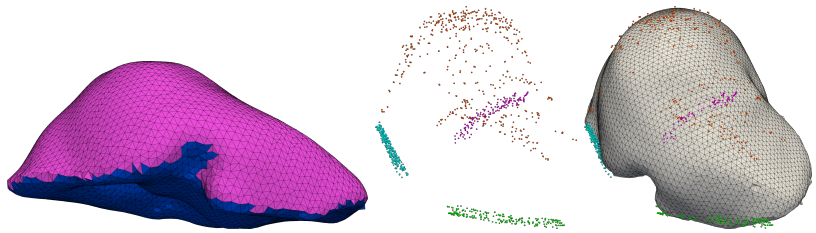

Fig. 1: Left: Initial liver mesh with matching surface on top and loaded surface in the bottom. Right: Point cloud and liver mesh after rigid registration

a linear elastic model for the liver phantom, with $E = 1$ and $\nu = 0.4$. The procedure is stopped after 200 iterations.

In Table 1, we reported the target registration error statistics for all datasets returned by the challenge website after submission of the results. Even for point clouds with a low surface coverage, the average target registration error stays below the 5 mm error that is usually required for clinical applications. In Figure 2, our results are compared with other submissions to the challenge. We obtained the second best result displayed on the challenge website (the first one is that of the challenge organizers), which shows that our approach is competitive for registration applications. No information about methods used by other teams is displayed on the challenge website.

Surface Coverage	Average	Standard deviation	Median
20-28 %	3.54	1.11	3.47
28-36 %	3.27	0.85	3.19
36-44 %	3.13	0.82	3.13
All data sets	3.31	0.94	3.19

Table 1: Target registration error statistics (in millimeters) for all datasets, as returned by the website after submission.

3.2 Force estimation in robotic surgery

Estimating the force applied by a robotic arm onto an organ is necessary to avoid causing damage to living tissues. As certain standard surgical robots are not equipped with force sensors, many indirect methods based on image processing have been proposed [13]. Here we estimate a force in a context similar to [9], where the intra-operative point cloud is estimated from a laparoscopic camera.

We generate 5 synthetic test cases using a liver mesh of 3,046 vertices and a linear elastic model ($E = 20,000$ Pa, $\nu = 0.45$). Dirichlet conditions are applied at the hepatic vein entry and in the falciform region. A test case is a sequence of traction forces applied onto two adjacent triangles on the anterior surface of

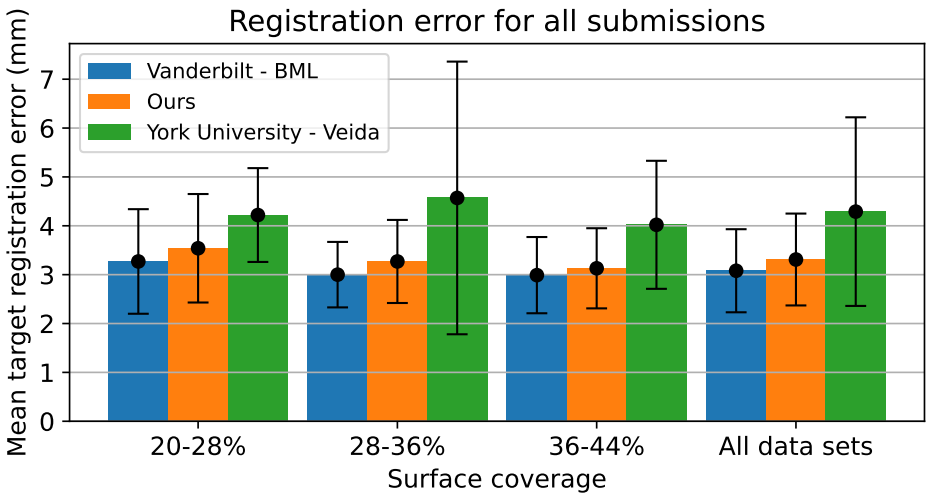

Fig. 2: Comparison of our TRE results with other participants to the challenge.

the liver to mimick the action of a robotic tool manipulating the liver. For each traction force, the resulting displacement is computed and a part of the deformed boundary is sampled to create a point cloud of 500 points. Each sequence consists of 50 forces, with a displacement of about 1 mm between two successive forces.

To avoid the inverse crime, we use a different mesh (3,829 vertices) for the registration, with the same linear elastic model as above. We allow the force distribution $\mathbf{b}$ to be nonzero only in a small zone (about 50 vertices) surrounding the triangles concerned by the traction force. In a clinical context, this approximate contact zone may be determined by segmenting the instrument tip on laparoscopic images. For a given traction force f_{true}, we solve the optimization problem with a relative tolerance of $5 \cdot 10^{-4}$ on the objective gradient norm and we compute the force estimation $f_{\text{est}} \in \mathbb{R}^3$ as the resultant of all the nodal forces of the reconstructed distribution $\mathbf{b}$. Then we compute the relative error $\|f_{\text{est}} - f_{\text{true}}\| / \|f_{\text{true}}\|$. Figure 3 shows the original synthetic deformation and the reconstructed deformation and surface force distribution.

For each sequence, the observed point clouds are successively fed to the procedure to update the force estimation by solving the optimization problem. The optimization algorithm is initialized with the last reconstructed distribution, so that only a few iterations are required for the update. Table 2 shows the average error obtained for each sequence, together with the average execution time of the updates and the number of evaluations of the objective function.

The noise in the reconstructed distribution results in an intensity smaller than the reference, which is the main cause of an overall error of 10 % in average. Note that the estimated force is proportional to the Young modulus of the model, which can be measured using elastography. According to [16], an error of 20 % is typical for clinical elastographic measurements. In this context, the elastographic

estimation is responsible for a larger part of the total error on the force estimation than our method.

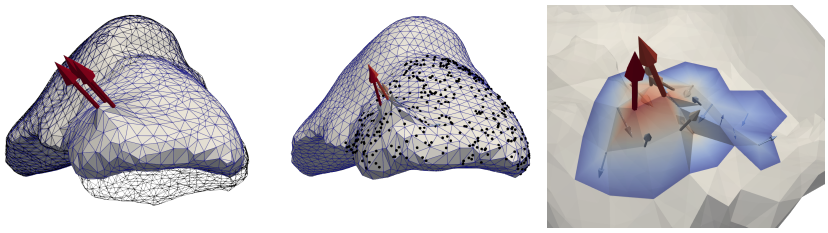

Fig. 3: Synthetic deformation generated by a local force (left), reconstructed deformation using the point cloud (center) and zoom on the reconstructed force field (right). Nodal forces are summed to produce a resultant estimation.

Sequence	N. eval.	Update Time	Relative error
Case 1	9.2	1.42 s	8.9 %
Case 2	5.6	0.85 s	16.2 %
Case 3	5.5	0.84 s	5.7 %
Case 4	5.4	0.82 s	4.4 %
Case 5	6.2	0.96 s	15.0 %

Table 2: Average number of objective evaluations, execution time per update and relative error for each sequence.

4 Conclusion

We presented a formulation of the liver registration problem using the optimal control formalism, and used it with success in two different application cases. We showed that we can not only reconstruct an accurate displacement field, but also, in certain cases, give a meaning to the optimal force distribution returned by the procedure. By tuning the formulation parameters (namely the set of admissible controls), we easily added new hypotheses into the direct model without changing the code of our procedure. These numerical results highlight the relevance and the flexibility of an optimal control approach in augmented surgery. Due to its mathematical foundations, the optimal control formalism is probably an important step toward provable accuracy for registration methods. Current limitations in our work include the lack of results with hyperelastic models due to their high computational cost. In the next steps of our work, we intend to reduce computation times by initializing the optimization process with the output of a neural network.

Bibliography

[1] Allaire, G.: Conception optimale de structures, Mathématiques & Applications (Berlin) [Mathematics & Applications], vol. 58. Springer-Verlag, Berlin (2007)

[2] Besl, P.J., McKay, N.D.: Method for registration of 3-D shapes. In: Schenker, P.S. (ed.) Sensor Fusion IV: Control Paradigms and Data Structures. vol. 1611, pp. 586 – 606. International Society for Optics and Photonics, SPIE (1992)

[3] Brewer, E.L., Clements, L.W., Collins, J.A., Doss, D.J., Heiselman, J.S., Miga, M.I., Pavas, C.D., III, E.H.W.: The image-to-physical liver registration sparse data challenge. In: Fei, B., Linte, C.A. (eds.) Medical Imaging 2019: Image-Guided Procedures, Robotic Interventions, and Modeling. vol. 10951, pp. 364 – 370. International Society for Optics and Photonics, SPIE (2019)

[4] Byrd, R.H., Lu, P., Nocedal, J., Zhu, C.: A limited memory algorithm for bound constrained optimization. SIAM Journal on Scientific Computing **16**(5), 1190–1208 (1995)

[5] Collins, J.A., Weis, J.A., Heiselman, J.S., Clements, L.W., Simpson, A.L., Jarnagin, W.R., Miga, M.I.: Improving registration robustness for image-guided liver surgery in a novel human-to-phantom data framework. IEEE Transactions on Medical Imaging **36**(7), 1502–1510 (2017)

[6] Delingette, H., Ayache, N.: Soft tissue modeling for surgery simulation. In: Computational Models for the Human Body, Handbook of Numerical Analysis, vol. 12, pp. 453–550. Elsevier (2004)

[7] Haouchine, N., Cotin, S., Peterlík, I., Dequidt, J., Lopez, M.S., Kerrien, E., Berger, M.: Impact of soft tissue heterogeneity on augmented reality for liver surgery. IEEE Transactions on Visualization and Computer Graphics **21**(5), 584–597 (2015)

[8] Haouchine, N., Dequidt, J., Peterlík, I., Kerrien, E., Berger, M., Cotin, S.: Image-guided simulation of heterogeneous tissue deformation for augmented reality during hepatic surgery. In: 2013 IEEE International Symposium on Mixed and Augmented Reality (ISMAR). pp. 199–208 (2013)

[9] Haouchine, N., Kuang, W., Cotin, S., Yip, M.: Vision-based force feedback estimation for robot-assisted surgery using instrument-constrained biomechanical three-dimensional maps. IEEE Robotics and Automation Letters **3**(3), 2160–2165 (2018)

[10] Heiselman, J.S., Jarnagin, W.R., Miga, M.I.: Intraoperative correction of liver deformation using sparse surface and vascular features via linearized iterative boundary reconstruction. IEEE Transactions on Medical Imaging **39**(6), 2223–2234 (2020)

[11] Marchesseau, S., Chatelin, S., Delingette, H.: Nonlinear biomechanical model of the liver. In: Payan, Y., Ohayon, J. (eds.) Biomechanics of Liv-

ing Organs, Translational Epigenetics, vol. 1, pp. 243–265. Academic Press, Oxford (2017)

[12] Miller, K., Joldes, G., Lance, D., Wittek, A.: Total lagrangian explicit dynamics finite element algorithm for computing soft tissue deformation. Communications in Numerical Methods in Engineering **23**(2), 121–134 (2007)

[13] Nazari, A.A., Janabi-Sharifi, F., Zareinia, K.: Image-based force estimation in medical applications: A review. IEEE Sensors Journal **21**(7), 8805–8830 (2021)

[14] Nesme, M., Payan, Y., Faure, F.: Efficient, Physically Plausible Finite Elements. In: Eurographics. Short papers, Dublin, Ireland (Aug 2005)

[15] Nikolaev, S., Cotin, S.: Estimation of boundary conditions for patient-specific liver simulation during augmented surgery. International Journal of Computer Assisted Radiology and Surgery **15**(7), 1107–1115 (May 2020)

[16] Oudry, J., Lynch, T., Vappou, J., Sandrin, L., Miette, V.: Comparison of four different techniques to evaluate the elastic properties of phantom in elastography: is there a gold standard? Physics in Medicine and Biology **59**(19), 5775–5793 (sep 2014)

[17] Özgür, E., Koo, B., Le Roy, B., Buc, E., Bartoli, A.: Preoperative liver registration for augmented monocular laparoscopy using backward–forward biomechanical simulation. International Journal of Computer Assisted Radiology and Surgery **13**(10), 1629–1640 (Oct 2018)

[18] Peterlík, I., Courtecuisse, H., Rohling, R., Abolmaesumi, P., Nguan, C., Cotin, S., Salcudean, S.: Fast elastic registration of soft tissues under large deformations. Medical Image Analysis **45**, 24–40 (2018)

[19] Plantefève, R., Peterlík, I., Haouchine, N., Cotin, S.: Patient-specific biomechanical modeling for guidance during minimally-invasive hepatic surgery. Annals of Biomedical Engineering **44**(1), 139–153 (Jan 2016)

[20] Rucker, D.C., Wu, Y., Clements, L.W., Ondrake, J.E., Pheiffer, T.S., Simpson, A.L., Jarnagin, W.R., Miga, M.I.: A mechanics-based nonrigid registration method for liver surgery using sparse intraoperative data. IEEE Transactions on Medical Imaging **33**(1), 147–158 (2014)

[21] Sahillioğlu, Y.: Recent advances in shape correspondence. The Visual Computer **36**(8), 1705–1721 (Aug 2020)

[22] Suwelack, S., Röhl, S., Bodenstedt, S., Reichard, D., Dillmann, R., dos Santos, T., Maier-Hein, L., Wagner, M., Wünscher, J., Kenngott, H., Müller, B.P., Speidel, S.: Physics-based shape matching for intraoperative image guidance. Medical Physics **41**(11), 111901 (2014)